JASA ARTICLE

Effects of a secondary high amplitude stimulus on the impedance of perforated plates

Ralf Burgmayer,[a] Friedrich Bake,[b] and Lars Enghardt
German Aerospace Center, Berlin 10623, Germany

ABSTRACT:
High sound pressure levels cause impedance changes in orifices and perforated plates due to vortex shedding and jet formation at the orifices. The effects of an additional high amplitude stimulus, unrelated in terms of frequency and phase, on the impedance of perforated plates received little attention. This work experimentally studies the impedance changes of perforated plates at various primary frequencies when an additional unrelated high-level single tone actuation is applied. It is shown that the impedance, the primary sound field faces, is altered dependent on the particle velocity induced in the orifices by the secondary actuation. Dimensionless quantities correlating the change of impedance with the secondary excitation are identified from the measurements and an empirical model for the change of resistance at quasi-steady flow conditions is derived. The results show that for low amplitude primary sound fields, the change of impedance is completely dependent on the secondary sound field. In case of a high amplitude primary sound field, the impedance is dependent on the particle velocities induced by both sound fields, whereas the larger induced particle velocity is the main contributor to the impedance changes. For unsteady flow conditions, a dependency on the frequency of the secondary actuation is found. https://doi.org/10.1121/10.0004951
(Received 11 January 2021; revised 16 April 2021; accepted 19 April 2021; published online 21 May 2021)
[Editor: David E. Scarborough] Pages: 3406–3415

I. INTRODUCTION

For low sound pressure levels, the impedance of perforated plates is only dependent on the geometric parameters of the perforated plates. For this so-called linear domain, a variety of models exist to calculate the impedance of perforated plates, e.g., Ref. 1. With rising sound pressure level, however, the impedance exhibits nonlinear behaviour due to flow separation and shows dependency on the particle velocity in the holes of the perforated plate. Several experimental studies were carried out on the nonlinear effects of orifices and perforated plates. Ingård and Labate[2] observed the formation of jets and vorticity shedding at the exit of an orifice. Acoustic energy is converted into kinetic energy of the vortices, leading to an increase in the resistance of the perforation. Ingård and Ising[3] found the resistance to increase linearly with the particle velocity in the orifice at high sound pressure levels. The behavior of the reactance is more complex and received less attention in the literature since the effects of the particle velocity on the reactance are comparably small when coupled to a cavity. The reactance decreases with increasing particle velocity and tends to an asymptotic limit of approximately one half of its linear value.[3] This is based on the assumption of irrotational flow at only the very side of the orifice where the flow is directed into the orifice. Various more or less empirical models exist that describe the nonlinear change of impedance under high sound pressure levels, e.g., Refs. 4–6. Bodén[7] studied the acoustic properties of perforated plates and orifices under high level multi tone excitation. While mostly focusing on harmonically related stimuli, he found a change of impedance at one frequency when varying the strength of excitation at another frequency. In contrast to previously conducted research, this work experimentally studies the impedance changes of perforated plates at a primary sound field due to, in terms of frequency and phase, an unrelated high amplitude secondary single tone actuation. Measurements of the change of impedance, induced by the secondary stimulus, are conducted and the results are correlated with dimensionless quantities. Thereby, both sound fields are varied in terms of amplitude and frequency. Particular focus is set on how the variation of actuation strength and frequency of the unrelated secondary stimulus affects the change of impedance of the perforated plate at the frequencies of the primary sound field.

II. THEORETICAL CONSIDERATIONS

Following the derivations of Kawell *et al.*,[8] the flow through an orifice, resulting from the interaction of two sound fields, can be described by a modified Bernoulli equation in the time domain. Note that the time dependency in Eqs. (1) and (3) has been omitted,

$$-\Delta(p_p + p_s) = p_p(0) + p_s(0) - (p_p(h) + p_s(h)) = \underbrace{\rho_0 L_{in}\frac{du}{dt}}_{Inertia} + \underbrace{\frac{1}{2C_d^2}\rho_0 u|u|}_{Convection} + \underbrace{\mu\left(\frac{\partial u}{\partial r}\right)_W \frac{4L_{res}}{d}}_{Friction}. \quad (1)$$

p_p represents the sound pressure of the primary sound field and p_s the sound pressure of the secondary sound field with

[a]Electronic mail: ralf.burgmayer@dlr.de
[b]ORCID: 0000-0002-3235-428X.

 0001-4966/2021/149(5)/3406/10/$30.00

https://doi.org/10.1121/10.0004951

their corresponding frequencies f_p and f_s. Respectively, $-\Delta(p_p + p_s)$ represents the pressure differential over the orifice of thickness h. ρ_0 is the density of air. $L_{in} = h + 2\Delta e_{in}$ is the effective inertial length and the sum of h and an inertial end correction Δe_{in}, multiplied by 2, accounting for fluid moving outside, on both sides of the orifice. Rayleigh showed the end correction for one side of the orifice to be $\Delta e_{in} = 4d/(3\pi)$.[9] $u = u_p + u_s$ is the effective spatially averaged particle velocity in the orifice and the sum of the particle velocities of the primary and secondary sound fields u_p and u_s in the orifice. The discharge coefficient C_d in the convective term is a function of time, as u changes over an oscillation period, and is dependent on the geometrical parameters of the plate: The orifice diameter d, h and the porosity σ. The third term on the right side represents a frictional correction term accounting for viscous losses, where $L_{res} = h + 2\Delta e_{res}$ is the resistive correction length and $(\partial u/\partial r)_W$ is the gradient of the particle velocity at the wall. At low particle velocities and for sharp edges, $e_{res} \approx e_{in}$. With increasing particle velocity amplitudes, the particle displacement is increasing and flow separation starts to occur as the displacement becomes comparable to the orifice dimensions. The ratio comparing orifice diameter to acoustic particle displacement is the Strouhal number defined as[10]

$$St = \frac{2\pi f d}{|u|}. \tag{2}$$

For $St \gg 1$, the convective contributions are negligible. For $1 \leq St \leq 5$, the flow conditions become unsteady and vortices form at the edges of the orifice, but no shedding occurs. For $St < 1$, the particle displacement exceeds the orifice dimensions, and flow separation arises. The flow can be assumed quasi-steady. Due to flow separation, L_{in} can be reduced by at least Δe_{in}. As the convective term becomes dominant, the friction term can be neglected. When $|u_p| \ll |u_s|$, the quadratic terms of $|u_p|$ can be neglected. Hence, under the assumption of independence of secondary and primary sound field, the resistance of the primary sound field solely faces flow separation effects due to $|u_s|$. Focusing on the primary sound field, Eq. (1) is written as

$$-\Delta p_p = \rho_0 L_{in}\frac{du_p}{dt} + \frac{1}{2C_d^2}\rho_0 u_p|u_s| + \mu\left(\frac{\partial u_s}{\partial r}\right)_W \frac{4L_{res}}{d}. \tag{3}$$

The effect of wall friction is approximated by the model for thin viscous boundary layers of Morse and Ingard.[11] Taking the Fourier transform of Eq. (3) under the assumption of $f_p \gg f_s$ yields

$$Z = i\rho_0\omega L_{in} + \frac{\rho_0|u_s|}{\pi C_d^2} + \sqrt{\mu\frac{\rho_0\omega}{2}}(1+i)\frac{4L_{res}}{d}, \tag{4}$$

where $Z = -\Delta p_p/u_p$ describes the acoustic impedance of a single orifice, the primary sound field is facing. Under the assumption of homogeneously distributed orifices, the impedance of a perforated plate is given by dividing Eq. (4) by σ. Based on a literature review,[3–5,12,13] we assume Z to be a function of ρ_0, c_0, d, h, σ, f_p, f_s, and the amplitudes of the root-mean-square (rms) particle velocities in the perforations, induced by the primary and secondary sound source $|\bar{u}_p|$ and $|\bar{u}_s|$. Using dimensional analysis, we express the dimensionless impedance $\zeta = Z/\rho_0 c_0$ as

$$\zeta = f\left(M_{ac}, \sigma, \frac{h}{d}, St_p, St_s, \frac{|\bar{u}_p|}{|\bar{u}_s|}\right), \tag{5}$$

where $M_{\mathrm{ac}} = |\bar{u}_s|/c_0$ is the acoustic Mach number for the secondary excitation. $St_p = 2\pi f_p d/|\bar{u}_s|$ and $St_s = 2\pi f_s d/|\bar{u}_s|$. Note that in this study, we define the Strouhal number in terms of the rms particle velocity $|\bar{u}|$ as it is approximately equal to the time averaged particle velocity for a harmonic excitation.

III. EXPERIMENTAL DESIGN

A. Experimental setup and analysis method

Figure 1 depicts the experimental setup. The setup consists of two identical rectangular duct sections, each of 80 mm width, 60 mm height, and 1550 mm length. We use four $\frac{1}{4}$ in. pressure microphones of type GRAS 40BP per section. Both sections are equipped with loudspeakers of type BMS 4599ND and weakly reflecting terminations in order to minimize standing waves in the duct. The reflection factor $r \leq 0.15$ for both terminations over the measured frequency range. The perforated plate, illustrated as a dashed line, is mounted between both sections at $x = 0$. Loudspeaker A (LS A) excites the primary sound field in Fig. 1, section 1 in a

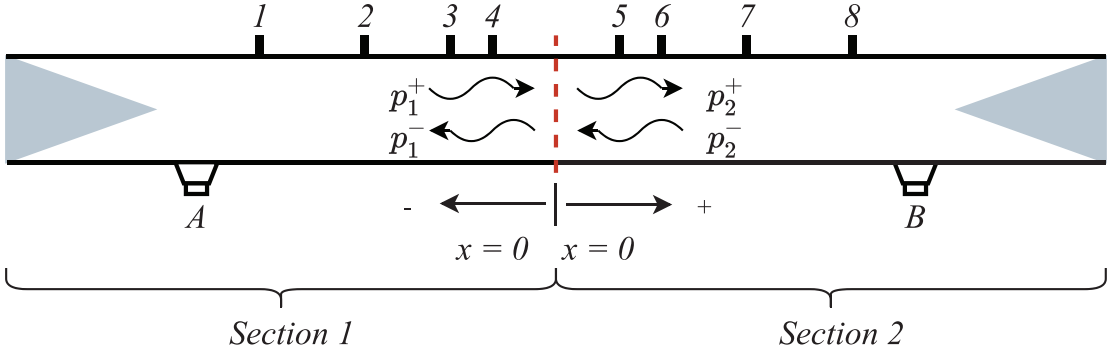

FIG. 1. (Color online) Schematic description of experimental setup.

frequency range from 200 to 1600 Hz with single tone stimuli in 51 Hz steps. LS B actuates a secondary high amplitude sound field in section 2. The secondary sound field is varied in amplitude and frequency: Single tone stimuli of two different frequencies $f_s = 331$ and $f_s = 943$ Hz are used. Both f_s are unrelated to the primary sound field frequencies f_p in terms of frequency and phase. To study possible differences resulting from linear and nonlinear primary sound fields, measurements are conducted for two different amplitudes, defined by the rms sound pressure level (SPL) of the incident plane wave: In the linear domain, the primary sound field is emitted with an incident plane wave SPL of $\bar{p}^+_{1,l} =$ 100 dB. The nonlinear primary sound field is adjusted to $\bar{p}^+_{1,nl} = 135$ dB. The specific values are determined empirically: $\bar{p}^+_{1,l}$ is found by successively decreasing the SPL, until the impedance of the plate with the lowest porosity (see Table I) is unaffected by the sound field. To specify $\bar{p}^+_{1,nl}$, we increase the incident SPL for the plates with high porosity until the impedance exhibits significant nonlinear effects. The overall sound field is transformed into the frequency domain. Under the assumption of negligible nonlinear propagation effects in the duct[14] and the sole propagation of plane waves, the frequency data is decomposed into forward and backward travelling wave components $\hat{p}^+$ and $\hat{p}^-$ by a plane wave decomposition in both sections separately.[15] Thermo-viscous damping is included by calculating the wave number k according to the model proposed by Dokumaci.[16] The complex amplitudes are used to calculate the impedance of the perforated plates and the corresponding peak particle velocity in the orifices. The specific impedance of the plate ζ is calculated for the frequencies of the primary sound field at $x = 0$ in section 1 of Fig. 1 and is given as

$$\zeta = \frac{\Delta p}{\rho_0 c_0 \hat{u}_p \sigma} = \frac{\hat{p}_1^+ + \hat{p}_1^- - \hat{p}_2^+ - \hat{p}_2^-}{\hat{p}_1^+ - \hat{p}_1^-}, \tag{6}$$

where $\hat{u}_p$ is derived from Euler's law and calculated from the plane wave components of the primary sound field at $x = 0$ in Fig. 1, section 1 under the assumption of continuity. $\hat{u}_s$ is calculated in the same manner from the wave components of the secondary sound field at $x = 0$ in Fig. 1, section 2,

$$\hat{u}_p = \frac{\hat{p}_1^+ - \hat{p}_1^-}{\rho_0 c_0 \sigma}, \tag{7a}$$

$$\hat{u}_s = \frac{\hat{p}_2^- - \hat{p}_2^+}{\rho_0 c_0 \sigma}. \tag{7b}$$

TABLE I. Geometric parameters of the perforated plates.

Sample	σ (%)	d (mm)	h (mm)
P1	1.03	1.5	1
P2	4.09	1.5	1
P3	4.09	2.5	1
P4	6.18	1.5	1
P5	6.18	1.5	2

Note that in addition to measurement equipment, nonlinear behavior of an orifice introduces higher harmonics, see, e.g., Ref. 17 for an in depth treatment. As the generation of higher harmonics was sufficiently low in the conducted measurements, the study is limited to the fundamental harmonic of the particle velocity. Measurement errors are assessed with randomly repeated measurement points. Results from repeated measurements exhibit deviations smaller than 3%.

B. Specifications of the samples

Table I gives an overview of the geometric parameters of the plates under study. The hole distribution is homogeneous and the hole geometry is circular for all specimens considered.

IV. RESULTS AND DISCUSSION

A. Resistance

1. Dimensionless control variables

With a primary sound field of low amplitude, we solely measure the change of resistance due to flow separation induced by the secondary excitation. The results are displayed as the difference of specific resistance $\mathrm{Re}\{\Delta\zeta\}$ when both sound fields act on the perforated plate $\mathrm{Re}\{\zeta\}$ compared to the specific resistance with only the primary sound field being present $\mathrm{Re}\{\zeta_p\}$. Furthermore, $\mathrm{Re}\{\Delta\zeta\}$ is divided by the Helmholtz number $He = d\pi f_p/c$ and multiplied by σ to approximately display the resistance of one orifice,

$$\mathrm{Re}\{\Delta\zeta\}_{He} = \frac{(\mathrm{Re}\{\zeta\} - \mathrm{Re}\{\zeta_p\}) \cdot \sigma}{He}. \tag{8}$$

Data analysis shows that the best correlation of $\mathrm{Re}\{\Delta\zeta\}_{He}$ is achieved for the parameter $1/St_p$. Figure 2 depicts $\mathrm{Re}\{\Delta\zeta\}_{He}$ of plate P1 plotted against $1/St_p$. As can be seen, the measurement results collapse. Hence, they can be correlated *via* the dimensionless quantity $1/St_p$. For $f_p \ll f_s$, the measured values of $\mathrm{Re}\{\Delta\zeta\}_{He}$ (+ symbols) deviate slightly from the trend of the remaining points. The deviations decrease with increasing $1/St_p$, i.e., $|\bar{u}_s|$ and will be discussed in detail in Secs. IV A 2 and IV A 3. For $1/St_p \leq 1$, $\mathrm{Re}\{\Delta\zeta\}_{He}$ shows a quadratic dependence upon the particle velocity $|\bar{u}_s|$. For $1/St_p > 1$, the relation becomes linear. This behavior was observed in several studies regarding the nonlinear impedance of perforated plates at single tone excitation.[10] However, the peculiarity is that the increase in resistance, seen at the primary sound field frequencies f_p, is induced by the unrelated secondary sound field due to flow separation.

2. Effects of the secondary stimulus on the particle velocity of the primary sound field

Figure 3 shows the particle velocity of the primary sound field $|\bar{u}_p|$ at different $1/St_s$. The local variations of $|\bar{u}_p|$ correspond to standing wave patterns in the duct. Two

https://doi.org/10.1121/10.0004951

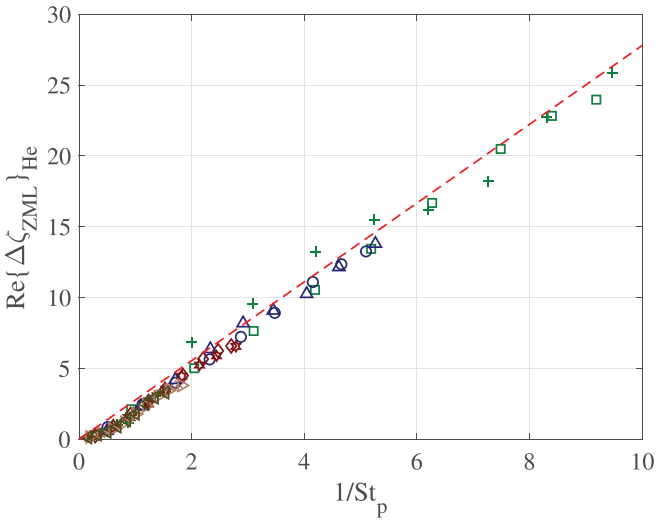

FIG. 2. (Color online) Sample P1: Change of resistance at $\bar{p}^{+}_{1,l} = 100$ dB plotted against dimensionless parameter $1/St_p$. Red dashed line: Eq. (13) (see Sec. IV A 3). Symbol reference:

	□	+	○	△	◇	▽	x	▷	*	◁
f_p [Hz]	255	255	459	459	867	867	1326	1326	1581	1581
f_s [Hz]	331	943	331	943	331	943	331	943	331	943

different effects can be seen: First, for low f_p, i.e., $f_p < f_s$ and low to medium $|\bar{u}_s|$, the excitation of the secondary sound field at different f_s yields different $|\bar{u}_p|$. This results in the small deviations of $\mathrm{Re}\{\Delta\zeta\}_{He}$ seen in Fig. 2 and can be explained by considering the ratio of secondary particle displacement to the orifice diameter, i.e., $1/St_s$ and the corresponding condition for the approximation of quasi-steady flow, $1/St_s > 1$: While quasi-stationary flow conditions are attained for $f_s = 331$ Hz for comparably low $|\bar{u}_s|$, for $f_s = 943$ Hz higher $|\bar{u}_s|$ have to be induced. When $1/St_s > 1$ for both f_s, as for the case of $1/St_s = 4.87$ at $f_s = 331$ Hz and $St_s = 1.67$ at $f_s = 943$ Hz, corresponding to $|\bar{u}_s| \approx 15$ m/s, the

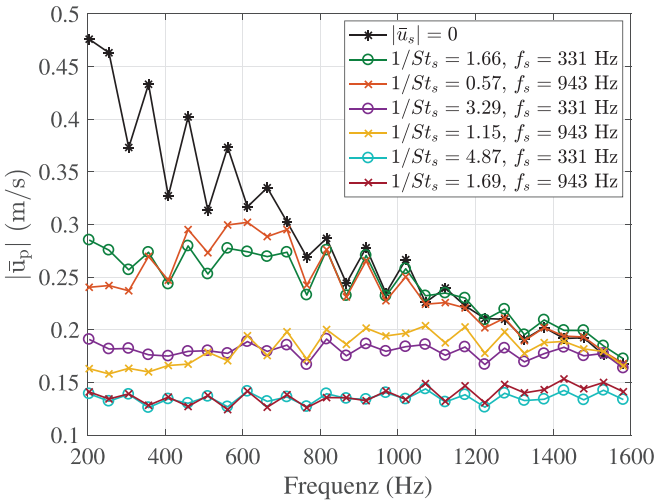

FIG. 3. (Color online) Sample P1: Particle velocity in the orifices induced by the primary sound source at $\bar{p}^{+}_{1,l} = 100$ dB for different $1/St_s$.

resulting $|\bar{u}_p|$ and hence $\mathrm{Re}\{\Delta\zeta\}_{He}$ become independent of f_s and coincide, as seen in Figs. 3 and 2. The dependency of $\mathrm{Re}\{\Delta\zeta\}_{He}$ on f_s for $1/St_s \leq 1$ will be discussed in detail in Sec. IV A 3. Second, as Bodén[7] showed, the effect of the secondary sound field is to reduce $|\bar{u}_p|$ by increasing the resistance of the perforates. Notably, the reduction of $|\bar{u}_p|$ is dependent on f_p. For $1/St_s = 1.66$ at $f_s = 331$ Hz and $1/St_s = 0.55$ at $f_s = 943$ Hz, corresponding to $|\bar{u}_s| \approx 5$ m/s, one can see, that for frequencies above $f_p \approx 800$ Hz, no reduction of $|\bar{u}_p|$ occurs. This corresponds to a limit of $1/St_p \approx 0.65$. For $1/St_p < 0.65$, the effect of the secondary particle velocity does not affect $|\bar{u}_p|$. Increasing the secondary particle velocity to $|\bar{u}_s| \approx 10$ m/s, i.e., $St_s = 3.29$ and $St_s = 1.15$, also increases the range of reduction from $|\bar{u}_p|$ to $f_p \approx 1600$ Hz. The limit is also seen in Fig. 2, as no significant change in resistance is seen below $1/St_p \approx 0.65$. For $1/St_s = 4.87$ at $f_s = 331$ Hz and $1/St_s = 1.69$ at $f_s = 943$ Hz, reduction of $|\bar{u}_p|$ is seen for all f_p studied. Above the limit, $|\bar{u}_p|$ is inversely proportional to $|\bar{u}_s|$, confirming the validity of the quasi-steady assumption in Eq. (4).

3. Effects of the secondary frequency

This section concerns the effects of the secondary frequencies on the resistance for $1/St_s \leq 1$. Figure 4 displays $\mathrm{Re}\{\Delta\zeta\}_{He}$ of P3 at $\bar{p}^{+}_{1,l} = 100$ dB. The ⋆ symbols depict results for frequency ratios $f_p/f_s > 1$, i.e., results, that are independent of f_s. Due to an increased orifice diameter $d = 2.5$ mm, the measurements at $f_s = 943$ Hz fall into the unsteady flow regime $0.2 \leq 1/St_s \leq 1$ of the secondary sound field. Deviations from the trend are seen for $f_p/f_s \ll 1$. Compared to Fig. 2, the magnitudes of deviations

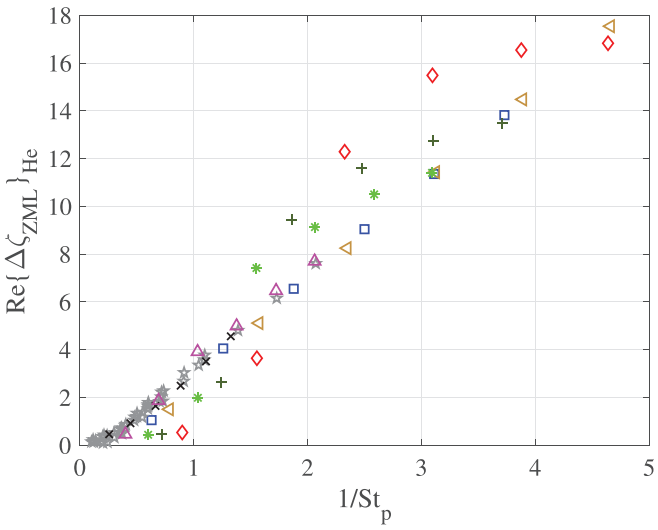

FIG. 4. (Color online) Sample P3: Change of resistance $\mathrm{Re}\{\Delta\zeta\}_{He}$ at $\bar{p}^{+}_{1,l} = 100$ dB. ⋆ Symbols: $\mathrm{Re}\{\Delta\zeta\}_{He}$ for $f_p/f_s \geq 1$. Symbol reference for $f_p/f_s < 1$:

	◇	+	*	△	x	▷	□
f_p [Hz]	204	255	306	459	716	204	255
f_s [Hz]	943	943	943	943	943	331	331

increase with d/h. The reason for the deviation is that the unsteady secondary sound field and hence the flow conditions through the orifice change fast with respect to the primary excitation: In extreme cases considered here, $|\bar{u}_s|$ cycles through four oscillation periods during one oscillation period of the primary sound field. The deviations decrease with increasing f_p/f_s, since the amount of variation of $|\bar{u}_s|$ over one oscillation period of the primary sound field decreases. The dependency on f_s becomes insignificant, when $f_p/f_s \geq 0.5$ ($\triangle$ symbols). Considering the results for $f_p/f_s < 0.5$ ($\diamond$, $+$, and $*$ symbols), maximum deviations occur, independent of $1/St_p$, at $|\bar{u}_s| = 9.92$ m/s, i.e., $1/St_s = 0.67$. Increasing $|\bar{u}_s|$, so that $1/St_s \approx 1$ results in decreasing dependency on f_s, as quasi-steady flow is approached for the secondary excitation. The same behavior, despite its negligible extent, can also be seen for $f_s = 331$ Hz ($\square$ and $\triangleleft$ symbols): The results at $1/St_p = 0.78$ and $1/St_p = 0.62$ correspond to measurements at $u_s = 2.52$ m/s, $f_p = 204$ Hz and $f_p = 255$ Hz, respectively, and hence, to $1/St_s = 0.48$. Increasing $|\bar{u}_s|$, yields agreement to the behavior of the results for $f_p \geq f_s$ because $1/St_s > 1$.

4. Variation of geometric parameters

The following considerations are limited to measurements where the quasi-steady approximation for the secondary excitation is valid, i.e., $1/St_s > 1$ or $f_p/f_s > 0.5$, respectively. Figure 5 shows $\mathrm{Re}\{\Delta\zeta\}_{He}$ for a variation of plate porosity at identical d / h. A slight increase in slope with increasing porosity is seen. The effect, despite its weak characteristic, can be attributed to flow separation effects due to the secondary actuation, since for low $1/St_p \leq 0.65$, the effect is not visible. We apply linear fits to the $\mathrm{Re}\{\Delta\zeta\}_{He}$ of different porosity for $1/St_p > 1$, where a linear relation to $|\bar{u}_s|$ is attained. Consequentially, we extract the slope parameter of the fits and in turn apply a linear fit to the extracted slopes in the logarithmic domain. The result is of the form: $fit_\sigma = 3.27\sigma^{0.051}$. The measurements are divided by fit_σ in order to study differences arising from a variation of the diameter to thickness ratio d/h with a soothed distortion by the effect of porosity.

Figure 6 shows the dependency of $\mathrm{Re}\{\Delta\zeta\}_{He,fit_\sigma}$ on d/h. The slope of $\mathrm{Re}\{\Delta\zeta\}_{He,fit_\sigma}$ increases with increasing d/h. The effect of d/h on the change of impedance is more pronounced than the effect of σ. After applying the same fitting process to the variation with d/h, we find $fit_{dh} = 0.94(d/h)^{0.33}$. Figure 7 shows the change of resistance for plates P3, P4, and P5 divided by the fits accounting for the variation with σ and d/h. As can be seen, a collapse of the measurement results is achieved.

By inspection of Fig. 7, one can deduce an empirical formulation to describe the change of resistance for $1/St_p > 1$ and $1/St_s > 1$, i.e., the convective term of Eq. (4),

$$\mathrm{Re}\{\Delta\zeta\}_{He,fit_{\sigma,dh}} \approx 1/St_p. \tag{9}$$

After solving for $\mathrm{Re}\{\Delta\zeta\}$ one receives

$$\mathrm{Re}\{\Delta\zeta\} = 3.08 \cdot \sigma^{0.05} \cdot \left(\frac{d}{h}\right)^{0.33} \cdot \frac{|\bar{u}_s|}{2c_0\sigma}. \tag{10}$$

For low porosities, Eq. (10) exhibits a resemblance to the commonly used term for the nonlinear resistance at single tone excitation, derived from the incompressible Bernoulli equation $R_{nl} = [u(1-\sigma^2)/2c_0\sigma C_d^2]$. For thin orifices $C_d \approx 0.61$.[15] The constant $C = 3.08$ is approximately equal to the term $1.15/C_d^2$. Consequently, we can write

$$Re\{\Delta\zeta\} = 1.15 \cdot \sigma^{0.051} \cdot \left(\frac{d}{h}\right)^{0.33} \cdot \frac{|\bar{u}_s|(1-\sigma^2)}{2c_0\sigma C_d^2}. \tag{11}$$

For $1/St_p \leq 1$, Eq. (11) is not valid due to the quadratic relation of $\mathrm{Re}\{\Delta\zeta\}_{He}$ to $|\bar{u}_s|$. The dependencies on the

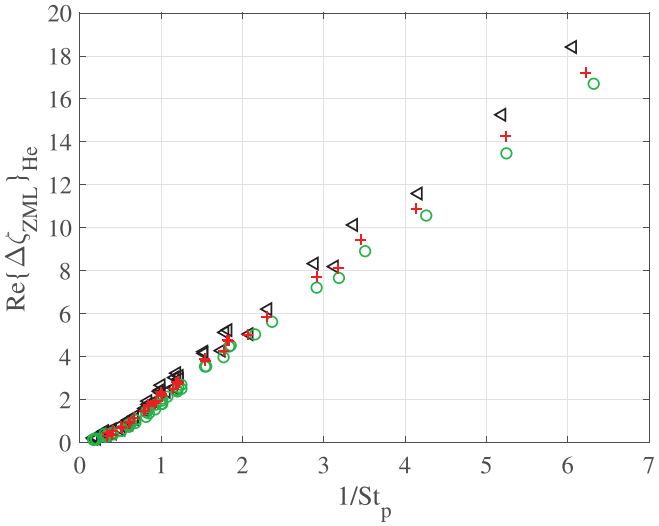

FIG. 5. (Color online) Effects of the variation of porosity on the change of resistance at $\bar{p}^+_{1,l} = 100$ dB. Samples P1 ($\bigcirc$, $\sigma = 1.03\%$), P2 ($+$, $\sigma = 4.09\%$), and P4 ($\triangleleft$, $\sigma = 6.18\%$).

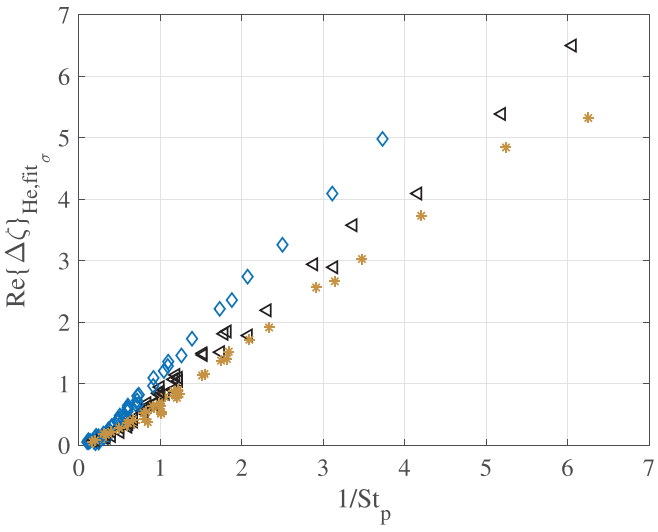

FIG. 6. (Color online) Effects of the variation of orifice-diameter-to-plate-thickness-ratios d/h on the change of resistance divided by fit for porosity $\mathrm{Re}\{\Delta\zeta\}_{He,fit_\sigma}$ at $\bar{p}^+_{1,l} = 100$ dB. Samples P3 ($\diamond$, $d/h = 2.5$), P4 ($\triangleright$, $d/h = 1.5$), and P5 ($*$, $d/h = 0.75$).

https://doi.org/10.1121/10.0004951

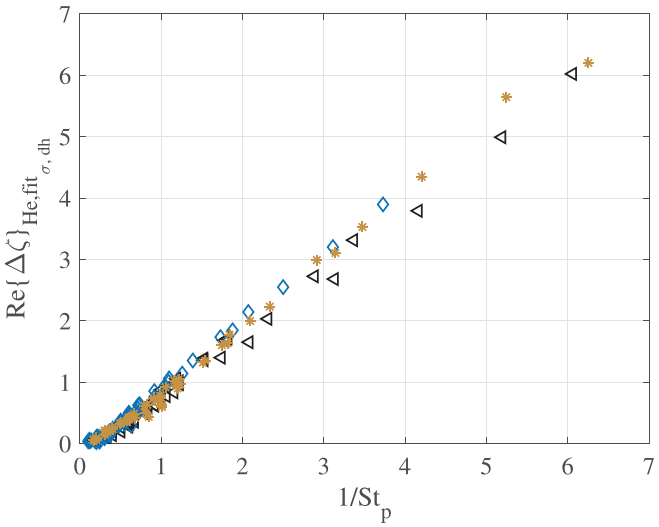

FIG. 7. (Color online) Change of resistance at $\bar{p}^+_{1,l} = 100$ dB divided by the fits accounting for geometric dependencies (fit_σ and fit_{dh}) for different orifice-diameter-to-plate-thickness-ratios and porosities. Samples P3 ($\diamond$, $d/h = 2.5$), P4 ($\triangleright$, $d/h = 1.5$), and P5 ($*$, $d/h = 0.75$).

geometrical parameters are related to C_d in Eq. (4). The acoustic discharge coefficient was found to change with excitation strength and frequency before plateauing at quasi-steady flow conditions. The plateau is dependent on the geometric parameters of the perforated plate. This is observed, among others, by Murray,[13] Zhou and Bodén,[18] and Hersh *et al.*[12] With

$$C_{d,nl} = \sqrt{\frac{C_d^2}{1.15 \cdot \sigma^{0.051} \cdot \left(\frac{d}{h}\right)^{0.33}}}, \tag{12}$$

Eq. (11) can be rewritten as

$$\mathrm{Re}\{\Delta\zeta\} = \frac{M_{ac}(1-\sigma^2)}{2\sigma C_{d,nl}^2}. \tag{13}$$

Figure 2 shows Eq. (13) divided by He compared to $\mathrm{Re}\{\Delta\zeta\}_{He}$ of P1 and shows good agreement for $1/St_p > 1$.

5. Nonlinear primary sound field

The implications of the interaction of two high amplitude sound fields on $\mathrm{Re}\{\Delta\zeta\}_{He}$ are discussed now. $\mathrm{Re}\{\Delta\zeta\}_{He}$ is defined in the same manner as in Sec. IV A 1 with the difference that the resistance $\mathrm{Re}\{\zeta_{p,nl}\}$ at $\bar{p}^+_{1,nl} = 135$ dB and $|\bar{u}_s| = 0$ is taken as reference

$$\mathrm{Re}\{\Delta\zeta\}_{He} = \frac{(\mathrm{Re}\{\zeta\} - \mathrm{Re}\{\zeta_{p,nl}\}) \cdot \sigma}{He}. \tag{14}$$

A high amplitude primary sound field causes nonlinearity due to flow separation at the perforated plate itself, i.e., $1/St_p \cdot |\bar{u}_p|/|\bar{u}_s| > 1$. This can be seen best for perforated plates with low porosity, where $|\bar{u}_p|$ reaches comparably high values. Thus, flow separation is attained for a wide range of f_p. Consequentially, the resistance increases and we find the applied $|\bar{u}_s|$ to be reduced. Compared to the case of a linear primary excitation, the effect of particle velocity reduction is reversed for $|\bar{u}_s| < |\bar{u}_p|$. The convective contributions to the resistance induced by both sound fields affect each other and the primary sound field suppresses the effect of the secondary actuation. Figure 8 shows $\mathrm{Re}\{\Delta\zeta\}_{He}$ of P1 for the high amplitude primary sound field ($\bar{p}^+_{1,nl} = 135$ dB) compared to the results for the linear primary sound field ($\bar{p}^+_{1,l} = 100$ dB, $\star$ symbols) plotted against $1/St_p$. The measurements for the two cases do not collapse, as the quadratic relation between $\mathrm{Re}\{\Delta\zeta\}_{He}$ and $1/St_p$ at $\bar{p}^+_{1,nl} = 135$ dB extends, dependent on f_p, to high values of $1/St_p$. Therefore, the usage of $1/St_p$ is not suited as characteristic flow parameter, when two high SPL signals interact at perforates. Nevertheless, the higher the frequency of the primary sound field f_p, the better the correlation of measurements at $\bar{p}^+_{1,nl} = 135$ dB and $\bar{p}^+_{1,l} = 100$ dB. This is because the flow separation due to the primary excitation decreases with increasing f_p. Thus, the resistance, the secondary sound field is subject to, is lower. Furthermore, the slopes of both measurements are similar. Based on these observations, we deduce the dimensionless control variable to be the difference function $1/St_{p,\Delta} = (|\bar{u}_s| - |\bar{u}_p|)/(2\pi f_p d)$. $1/St_{p,\Delta}$ can be negative for low $|\bar{u}_s|$. Figure 9 shows that the results for both primary sound field cases collapse, when plotted against the parameter $1/St_{p,\Delta}$. As soon as $1/St_{p,\Delta} \geq 0$, an increase in resistance is seen. For $0 \leq 1/St_{p,\Delta} \leq 1$, the relationship of the control variable and $\mathrm{Re}\{\Delta\zeta\}_{He}$ is quadratic. A linear relation is attained for $1/St_{p,\Delta} > 1$. The suppression

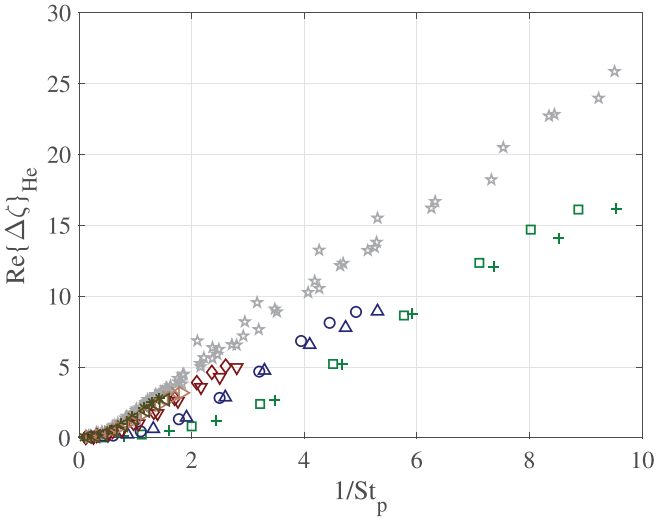

FIG. 8. (Color online) Sample P1: Change of resistance at $\bar{p}^+_{1,nl} = 135$ dB compared to the change of resistance at $\bar{p}^+_{1,l} = 100$ dB ($\star$) plotted against $1/St_p$. Symbol reference for the case $\bar{p}^+_{1,nl} = 135$ dB:

	□	+	○	△	◇	▽	x	▷	*	◁
f_p [Hz]	255	255	459	459	867	867	1326	1326	1581	1581
f_s [Hz]	331	943	331	943	331	943	331	943	331	943

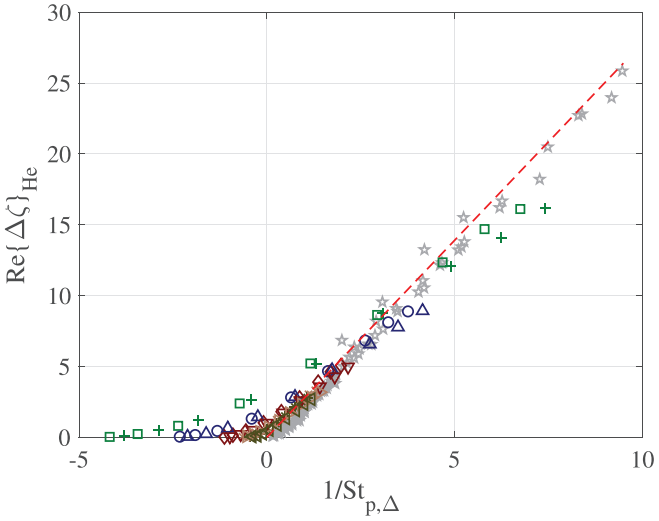

FIG. 9. (Color online) Sample P1: Change of resistance at $\bar{p}^+_{1,nl} = 135$ dB compared to the change of resistance at $\bar{p}^+_{1,l} = 100$ dB ($\star$) plotted against $1/St_{p,\Delta}$. Red dashed line: Eq. (15). Symbol reference for the case $\bar{p}^+_{1,nl} = 135$ dB:

	□	+	○	△	◇	▽	x	▷	*	◁
f_p [Hz]	255	255	459	459	867	867	1326	1326	1581	1581
f_s [Hz]	331	943	331	943	331	943	331	943	331	943

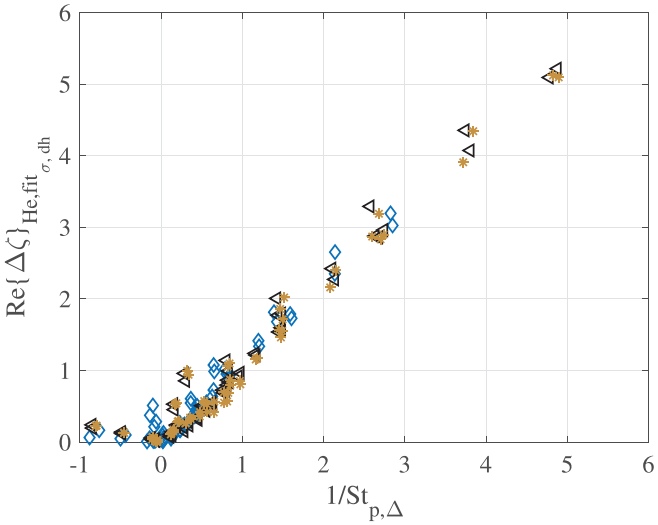

FIG. 10. (Color online) Change of resistance at $\bar{p}^+_{1,nl} = 135$ dB divided by the fits accounting for geometric dependencies. Samples P3 ($\diamond$, $d/h = 2.5$), P4 ($\triangleleft$, $d/h = 1.5$), and P5 ($*$, $d/h = 0.75$).

of the resistance change due to the secondary sound source is evident: The convective contributions of the secondary actuation have a negligible effect on the resistance of the perforated plate until the induced secondary particle velocity exceeds the primary particle velocity. The findings agree with the observations for the resistance of an orifice under high amplitude acoustic excitation and steady bias flow:[14] As soon as the acoustic particle velocity exceeds the bias flow velocity, the resistance changes with respect to the acoustic velocity. Furthermore, the unsteadiness of the flow is mitigated by high acoustic excitation. Here, the unsteady behavior for $f_p \ll f_s$, reported for the linear primary sound field (see Fig. 2), is also decreased. This is due to the fact, that for low f_p, quasi-steady flow conditions are attained by the primary excitation. For f_p, with $f_p/f_s > 0.5$ there is only negligible dependency on f_s, as shown in Sec. IV A 3. From the observations made in this section, it is concluded that since the primary sound field induces flow separation in the orifices as well, its effects on the impedance cannot be neglected. A significant increase in resistance due to the secondary actuation is found for $1/St_{p,\Delta} \geq 0$. Hence, convective contributions from the secondary sound field only need to be considered if $|\bar{u}_s|$ exceeds $|\bar{u}_p|$.

Figure 10 depicts $\mathrm{Re}\{\Delta\zeta\}_{He}$ for P3 ($\diamond$), P4 ($\triangleleft$), and P5 ($*$), divided by the fits accounting for geometric dependencies, derived in Sec. IV A 3. The collapse of results shows that the dependencies on d/h and σ are retained in the case of a high SPL primary sound field. Consequentially, Eq. (13) is rewritten as

$$\mathrm{Re}\{\Delta\zeta\} = \frac{(|\bar{u}_s| - |\bar{u}_p|)\cdot(1-\sigma^2)}{2\cdot c_0\cdot\sigma\cdot C^2_{d,nl}}; \quad if\ 1/St_{p,\Delta} > 1, \tag{15a}$$

$$\mathrm{Re}\{\Delta\zeta\} = 0; \quad if\ |\bar{u}_s| \leq |\bar{u}_p|. \tag{15b}$$

Compared to Eq. (13) where $|\bar{u}_p|$ could be neglected, Eq. (15) represents the general form of the change of resistance due to a high amplitude secondary sound field. Figure 9 shows a comparison of Eq. (15) divided by He to the measurements of P1. In general, Eq. (15) shows good agreement. At low f_p, $0 < 1/St_{p,\Delta} \leq 1$ deviations occur due to the quadratic relation of $\mathrm{Re}\{\Delta\zeta\}_{He}$ to $1/St_{p,\Delta}$.

B. Reactance

1. Linear primary sound field

The change of specific reactance is depicted as the ratio of the reactance, with a secondary excitation present, to the reactance, when only the primary sound field is active $Im\{\zeta\}/Im\{\zeta_p\}$. This can be interpreted as the ratio of end correction under secondary flow separation to the end correction without a secondary excitation present. Figure 11 shows $Im\{\zeta\}/Im\{\zeta_p\}$ of P3 plotted against $1/St_p$ for a primary sound field with $\bar{p}^+_{1,l} = 100$ dB. Compared to the resistance, enhanced deviating behavior is seen for $f_p \ll f_s$ (+, $*$, △ symbols): The smaller f_p/f_s becomes, the larger the deviations, and the deviations increase with increasing d/h. For $1/St_p < 1$, the end correction is increased as $(Im\{\zeta\}/Im\{\zeta_p\}) > 1$. The measurements correspond to $|\bar{u}_s| = 2.88$ m/s and $1/St_s = 0.19$ and hence to the onset of vortex formation due to the secondary excitation. The maximum deviations for P3 at $f_s = 943$ Hz are, analogous to the resistance, independent of $1/St_p$ and found for $1/St_s = 0.67$, i.e., at $|\bar{u}_s| = 9.92$ m/s. In this range of $1/St_s$, the end

https://doi.org/10.1121/10.0004951

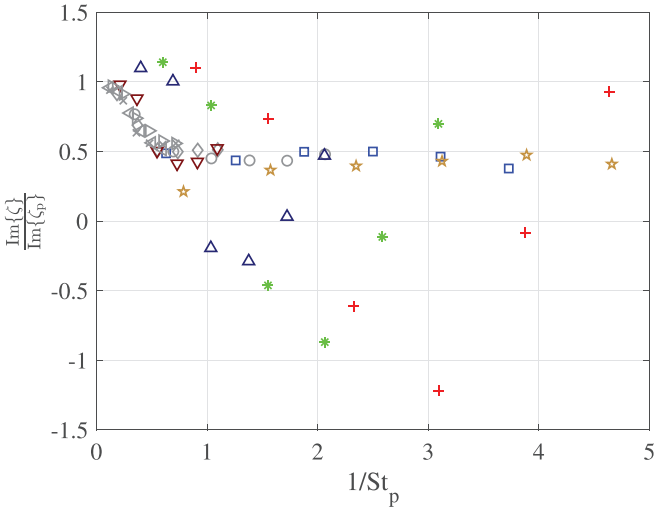

FIG. 11. (Color online) Sample P3: Change of reactance at $\bar{p}^{+}_{1,l} = 100$ dB. Symbol reference:

	⋆	+	□	∗	○	△	◇	▽	x	▷	◁
f_p [Hz]	204	204	255	306	459	459	867	867	1326	1326	1581
f_s [Hz]	331	943	331	943	331	943	331	943	331	943	943

corrections for $f_p/f_s \ll 1$ are negative. This is observed, in extreme cases, for orifices under bias flow[19] as well. Increasing $|\bar{u}_s|$ and hence $1/St_s$ further, quasi-steady behavior is approached for the secondary excitation, and the dependency on f_s decreases. This can be seen for $f_p/f_s = 0.61$ (⋆): At $1/St_p = 0.79$, corresponding to a measurement at $|\bar{u}_s| = 2.52$ ms, $f_s = 331$ Hz and $1/St_s = 0.48$, we see slight deviations, that vanish with increasing $|\bar{u}_s|$. For $f_p/f_s = 0.92$ (▽ symbols) the deviations from the trend are negligible. The remaining measurement points, i.e., $f_p/f_s \geq 1$, are independent of f_s and follow the same trend: For $0 \leq 1/St_p \leq 0.25$, the reactance is independent of $|\bar{u}_s|$ and no significant change is visible. For $0.25 < 1/St_p < 1$, the transition to quasi-steady flow conditions take place and the reactance decreases until a plateau value at a ratio of about $Im\{\zeta\}/\,Im\{\zeta_p\} \approx 0.5$ is attained.

For the analysis of the effects of variation of the geometrical parameters, the results for $f_p \ll f_s$ are excluded. Figure 12 shows the behavior of the reactance for different σ at identical ratios of d/h. The attained plateau level for $1/St_p > 1$ is decreasing with increasing σ. Figures 13 and 14 depict the difference in reactance with varying d/h at identical porosities. Figure 13 shows $Im\{\zeta\}/Im\{\zeta_p\}$ for $d/h = 1.5$ (+ symbols) and $d/h = 2.5$ (◇ symbols) at $\sigma = 4.09$ %. For $d/h = 2.5$, the rate of decrease is higher compared to $d/h = 1.5$, i.e., the plateau is attained for lower $1/St_p$. A small difference in plateau level can also be seen. Figure 14 shows the difference in $Im\{\zeta\}/Im\{\zeta_p\}$ for $d/h = 1.5$ (◁ symbols) and $d/h = 0.75$ (∗ symbols) at $\sigma = 6.18$ %. While for $d/h = 1.5$, the decrease in $Im\{\zeta\}/Im\{\zeta_p\}$ is rapid and limited to a small range of $1/St_p$, the decrease in $Im\{\zeta\}/Im\{\zeta_p\}$ for $d/h = 0.75$ extends up to $1/St_p > 1$.

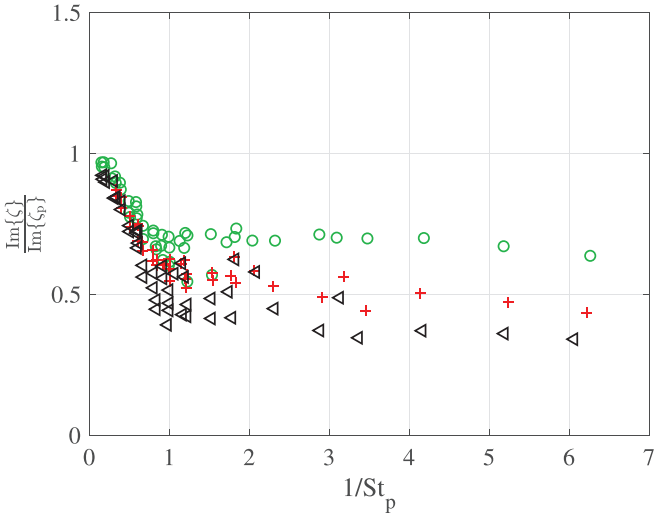

FIG. 12. (Color online) Change of reactance at $\bar{p}^{+}_{1,l} = 100$ dB with varying porosity. Samples P1 (○, $\sigma = 1.03\%$), P2 (+, $\sigma = 4.09\%$), and P4(◁, $\sigma = 6.18\%$).

Furthermore, there is a significant difference in the attained plateau values: The decrease in reactance is less for $d/h = 0.75$. From the observations made, one can conclude: The reactance shows dependency on f_s for $f_p < f_s$ and $0.2 \leq 1/St_s \leq 1$ due to unsteady flow conditions of the secondary actuation. When the secondary flow approaches quasi-steady conditions, i.e., $1/St_s \geq 1$, the dependency on f_s decreases. Furthermore, a dependency on the geometric parameters of the orifice plates are found. If $f_p \geq f_s$ or $1/St_s > 1$, the reactance decreases until a plateau is attained at $1/St_p > 1$.

2. Nonlinear primary sound field

Figure 15 shows the change of reactance of P3, for the case of a primary sound field at $\bar{p}^{+}_{1,nl} = 135$ dB plotted

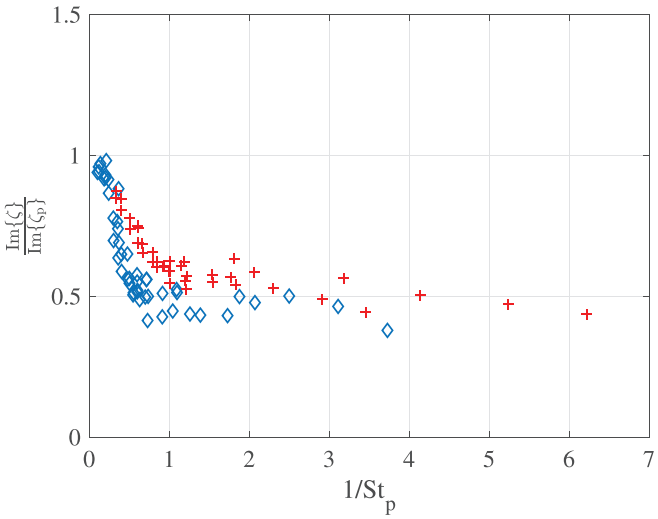

FIG. 13. (Color online) Change of reactance at $\bar{p}^{+}_{1,l} = 100$ dB with varying orifice-diameter-to-plate-thickness-ratio. Samples P2 (+, $d/h = 1.5$) and P3 (◇, $d/h = 2.5$).

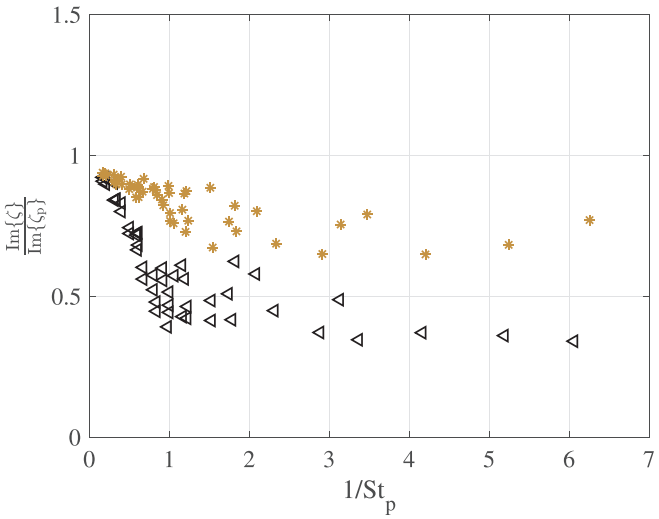

FIG. 14. (Color online) Change of reactance at $\bar{p}^+_{1,l} = 100$ dB with varying orifice-diameter-to-plate-thickness-ratio. Samples P4 ($\lhd$, $d/h = 1.5$) and P5 ($*$, $d/h = 0.75$).

against $1/St_p$. The data is depicted as the ratio of the reactance at $\bar{p}^+_{1,nl} = 135$ dB, with a secondary excitation present, to the reactance, when only the primary sound field at $\bar{p}^+_{1,l} = 100$ dB is active $Im\{\zeta\}/Im\{\zeta_p\}$. For medium and high f_p, the reactance measured at $\bar{p}^+_{1,nl} = 135$ dB and $\bar{p}^+_{1,l} = 100$ dB ($\star$ symbols) behaves similarly. Since flow separation is not attained by the primary excitation, i.e., $(|\bar{u}_p|/\,2\pi f_p d) \leq 1$, its effects can be neglected. For $f_p < f_s$, compared to the measurements at $\bar{p}^+_{1,l} = 100$ dB, the dependency on f_s is reduced. The range of $1/St_p$, where the deviations from the frequency independent behavior due to unsteady flow conditions of the secondary excitation occur, is shifted to higher values. This due to the increased influence of flow separation by the primary excitation at low f_p. Figure 16 shows a comparison of measurements for $f_p < f_s$ at $\bar{p}^+_{1,nl} = 135$ dB and $\bar{p}^+_{1,l} = 100$ dB plotted against $1/St_{p,\Delta}$. The $\star$ symbols depict measurements at $\bar{p}^+_{1,l} = 100$ dB and $f_p > f_s$. Since $(|\bar{u}_p|/2\pi f_p d) > 1$ for the measurements at $\bar{p}^+_{1,nl} = 135$ dB, the results (+ and x symbols) are at plateau level without secondary excitation active and independent of the secondary actuation for $1/St_{p,\Delta} \leq 0$. For $1/St_{p,\Delta} > 0$, despite being mitigated, the deviations occur at similar $1/St_{p,\Delta}$ as the corresponding measurements at $\bar{p}^+_{1,l} = 100$ dB ($\bigcirc$ and $\diamond$ symbols). For $f_p/f_s = 0.38$ at $f_s = 943$ Hz (+ symbols), we find $|\bar{u}_s| - |\bar{u}_p| = 8.58$ m/s at $1/St_{p,\Delta} = 1.53$ and hence $1/St_{s,\Delta} = |\bar{u}_s| - |\bar{u}_p|/2\pi f_s d = 0.58$. This corresponds to $1/St_s$ for the maximum deviations at $\bar{p}^+_{1,l} = 100$ dB found in Secs. IV A 3 and IV B 1. Increasing $|\bar{u}_s|$ further, so that $1/St_{s,\Delta} \approx 1$, independent behavior of f_s is approached. This is seen at $1/St_{p,\Delta} = 2.07$ corresponding to $|\bar{u}_s| - |\bar{u}_p| = 11.58$ m/s and $1/St_{s,\Delta} = 0.78$. The reactance at $f_p/f_s = 0.61$ ($f_s = 331$ Hz, x symbols) behaves similar and shows a slight dip at $1/St_{p,\Delta} = 0.74$, corresponding to $|\bar{u}_s| - |\bar{u}_p| = 2.36$ m/s and $1/St_{s,\Delta} \approx 0.45$. Increasing $|\bar{u}_s|$ leads to $1/St_{s,\Delta} > 1$ and independence of f_s. Equivalent behavior is found for the reactance under high amplitude acoustic excitation and bias flow:[14] The reactance under bias flow approximates the results without bias flow when the acoustic velocity is considerably larger than the bias flow velocity. This corresponds to $1/St_{s,\Delta} \approx 1$. When the acoustic particle velocity is comparable to the bias flow velocity, unsteady

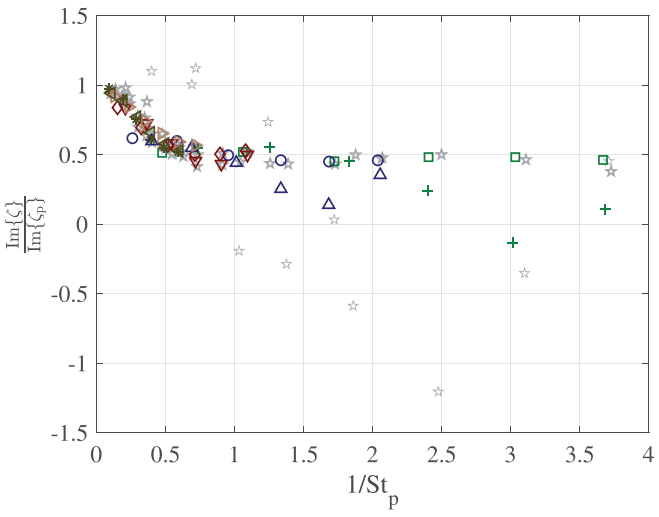

FIG. 15. (Color online) Sample P3: Change of reactance at $\bar{p}^+_{1,nl} = 135$ dB compared to $\bar{p}^+_{1,l} = 100$ dB ($\star$). Symbol reference for the case $\bar{p}^+_{1,nl} = 135$ dB:

	□	+	○	△	◇	▽	x	▷	*	◁
f_p [Hz]	255	255	459	459	867	867	1326	1326	1581	1581
f_s [Hz]	331	943	331	943	331	943	331	943	331	943

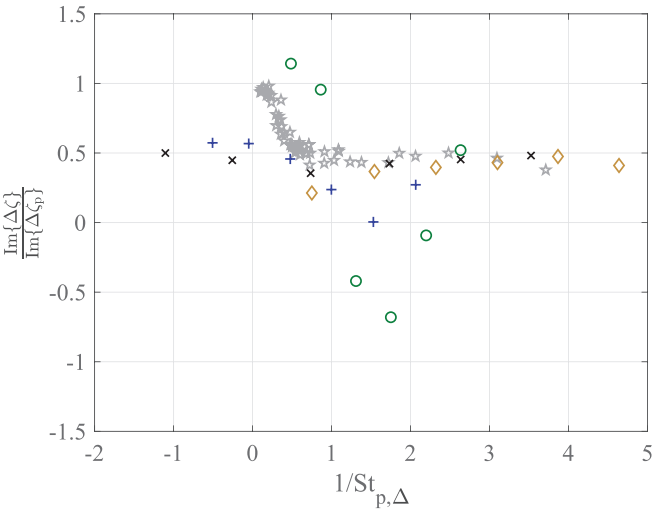

FIG. 16. (Color online) Sample P3: Comparison of the change of reactance at primary frequencies $f_p < f_s$ for $\bar{p}^+_{1,nl} = 135$ dB and $\bar{p}^+_{1,l} = 100$ dB. $\star$ symbols: Change of reactance at $\bar{p}^+_{1,l} = 100$ dB and $f_p >$ fs. Symbol reference for $f_p < f_s$:

	+	○	x	◇
$\bar{p}^+_1$ [dB]	135	100	135	100
f_p [Hz]	357	357	204	204
f_s [Hz]	943	943	331	943

https://doi.org/10.1121/10.0004951

behavior is observed. This is analogous to the results for $0.2 \leq 1/St_{s,\Delta} \leq 1$ found here.

V. CONCLUSION

This paper experimentally studies the effects of two unrelated sound fields interacting on the impedance of perforated plates. Particular interest is given to the change of impedance a primary sound field is facing due to the amplitude and frequency of an additional unrelated secondary sound field. It is demonstrated that, by means of flow separation induced by the secondary excitation, the impedance of perforated plates, impacting the primary sound field, is altered. This could be of potential use for the optimization of the damping capabilities of Helmholtz resonator liners. Dimensionless quantities, correlating the change of impedance with the secondary excitation, and conditions, permitting the use of quasi-steady assumptions, are identified. Consequentially, an empirical model for the change of resistance in the quasi-steady flow regime is derived from the measurements. For a low amplitude primary sound field, the primary particle velocity can be neglected and the change of impedance is only dependent on the particle velocity induced in the orifices by the secondary sound field. For unsteady flow conditions and primary frequencies smaller than the secondary frequency, a dependency of the impedance on the secondary frequency is found. As soon as the secondary particle displacement exceeds the orifice dimensions, frequency independence is attained. For a high amplitude primary sound field, flow separation is induced by both sound fields and, consequentially, the impedance is a function of both. A change of impedance due to the secondary actuation is obtained only if the secondary particle velocity exceeds the primary particle velocity. Moreover, the dependency on the secondary sound field frequency is reduced. As this dependency is not understood yet, the subject deserves further research.

ACKNOWLEDGMENTS

This study is supported by the project ARTEM (Aircraft noise Reduction Technologies and related Environmental iMpact) which has received funding from the European Union's Horizon 2020 research and innovation programme under Grant No. 769 350.

[1]N. Atalla and F. Sgard, "Modeling of perforated plates and screens using rigid frame porous models," J. Sound Vib. **303**, 195–208 (2007).
[2]K. U. Ingård and S. Labate, "Acoustic circulation effects and the nonlinear impedance of orifices," J. Acoust. Soc. Am. **22**, 211–218 (1950).
[3]K. U. Ingård and H. Ising, "Acoustic nonlinearity of an orifice," J. Acoust. Soc. Am. **42**, 6–17 (1967).
[4]T. H. Melling, "The acoustic impedance of perforates at medium and high sound pressure levels," J. Sound Vib. **29**, 1–65 (1973).
[5]R. Tayong, T. Dupont, and P. Leclaire, "On the variations of acoustic absorption peak with particle velocity in micro-perforated panels at high level of excitation," J. Acoust. Soc. Am. **127**, 2875–2882 (2010).
[6]Z. Laly, N. Atalla, and S.-A. Meslioui, "Acoustical modeling of micro-perforated panel at high sound pressure levels using equivalent fluid approach," J. Sound Vib. **427**, 134–158 (2018).
[7]H. Bodén, "Acoustic properties of perforates under high level multi-tone excitation," in *Proceedings of the 19th AIAA/CEAS Aeroacoustics Conference*, Germany, Berlin (May 27–29, 2013).
[8]S. T. Kawell, D. E. Stubbs, and D. C. Scarborough, "A theoretical investigation of the nonlinear acoustic response of abrupt area contractions," J. Acoust. Soc. Am. **147**, 500–507 (2020).
[9]J. W. Rayleigh, *The Theory of Sound* Vol. II (Macmillan, New York, 1894), p. 183.
[10]M. A. Temiz, J. Tournadre, I. L. Arteaga, and A. Hirschberg, "Non-linear acoustic transfer impedance of micro-perforated plates with circular orifices," J. Sound Vib. **366**, 418–428 (2016).
[11]P. M. Morse and K. U. Ingård, *Theoretical Acoustics* (Princeton University Press, Princeton, NJ, 1968).
[12]A. S. Hersh, B. E. Walker, and J. W. Celano, "Helmholtz resonator impedance model, part 1: Nonlinear behavior," AIAA J. **41**(5), 795–808 (2003).
[13]P. B. Murray and R. J. Astley, "Development of a single degree of freedom perforate impedance model under grazing flow and high SPL," in *Proceedings of the 18th AIAA/CEAS Aeroacoustics Conference (33th AIAA Aeroacoustics Conference)*, Colorado Springs, CO (June 4–6, 2012).
[14]L. Zhou and H. Bodén, "Experimental investigation of an in-duct orifice with bias flow under medium and high level acoustic excitation," Int. J. Spray Combust. Dyn. **6**, 267–292 (2014).
[15]C. Lahiri, "Acoustic performance of bias flow liners in gas turbine combustors," Ph.D. thesis, Technical University Berlin, Berlin, Germany (2013).
[16]E. Dokumaci, "Sound transmission in narrow pipes with superimposed uniform mean flow and acoustics modelling of automobile catalytic converters," J. Sound Vib. **182**, 799–808 (1995).
[17]N. S. Dickey and A. Selamet, "Acoustic nonlinearity of a circular orifice: An experimental study of the instantaneous pressure/flow relationship," Noise Control Eng. J. **46**(3), 97–107 (1998).
[18]L. Zhou and H. Bodén, "The effect of combined high level acoustic excitation and bias flow on the acoustic properties of an in-duct orifice," in *Proceedings of the 19th AIAA/CEAS Aeroacoustics Conference*, Germany, Berlin (May 27–29, 2013).
[19]E. Moers, D. Tonon, and A. Hirschberg, "Strouhal number dependency of the aero-acoustic response of wall perforations under combined grazing-bias flow," J. Sound Vib. **389**, 292 (2017).